Int. J. Heat Mass Transfer. Vol. 26, No. 1, pp. 109-120, 1983
Printed in Great Britain

0017-9310/83/010109-12 $03.00/0
Pergamon Press Ltd.

THE LONGITUDINAL VORTEX AND ITS EFFECTS ON THE TRANSPORT PROCESSES IN COMBINED FREE AND FORCED LAMINAR CONVECTION BETWEEN HORIZONTAL AND INCLINED PARALLEL PLATES

KEISUKE FUKUI and MASAMOTO NAKAJIMA
Department of Chemical Engineering, Himeji Institute of Technology, 671-22 Himeji, Japan

and

HIROMASA UEDA
National Institute for Environment Studies, P.O. Yatabe, Tsukuba, 305 Ibaraki, Japan

(*Received* 12 *January* 1982)

Abstract — The longitudinal vortex and its effects on transport processes in laminar flow between horizontal and inclined parallel-plates kept at different temperatures were investigated. A new set of experimental data is presented on the velocity and temperature fields. Theoretical predictions were made by means of a numerical finite-difference method. Based on good agreement between theory and experiment, the disturbed primary-flow fields along with the disturbance patterns were examined both for the horizontal and inclined flows. The maximum inclination angle was 32.1° from the horizontal and the Rayleigh numbers were less than 9300. It was shown that the interaction between vortices was rather small in the horizontal flow, the velocity-peak being near the vortex center. However, in the inclined flow, disturbance patterns changed remarkably; two neighboring vortices tended to form a pair which had a single velocity peak at the upwelling-boundary of the vortex in the upward flow, and conversely at the downwelling-boundary in the downward flow. Augmentations of the Nusselt number and pressure drop due to the vortex formation were shown to be independent of the inclination angle and were formulated in a simple form.

NOMENCLATURE

a_μ, a_λ, constants defined by equation (13);
b, distance between parallel plates [m];
c_p, specific heat at constant pressure [J kg^{-1} K^{-1}];
f, friction factor, $2|\tau_w|/\rho\langle u^*\rangle^2$;
Gr, Grashof number, $g\beta\Delta T^* b^3/\nu^2$;
g, gravitational acceleration [m s^{-2}];
h, dimensionless grid spacing;
M, N, number of grid lines in y and z directions, respectively;
Nu, Nusselt number, $|q|b/(\Delta T^*\lambda)$;
p^*, static pressure at the cooled wall [Pa];
p_0^*, static pressure at center of the fluid layer [Pa];
Pr, Prandtl number, $c_p\mu/\lambda$;
q, heat flux [J m^{-2} s^{-1}];
Ra, Rayleigh number, $Pr\,Gr$;
Re, Reynolds number, $\langle u^*\rangle b/\nu$;
T^*, temperature [K];
ΔT^*, temperature difference, $T_H^* - T_C^*$ [K];
u^*, v^*, w^*, velocity components (Fig. 1) [m s^{-1}];
x^*, y^*, z^*, coordinates (Fig. 1) [m].

Greek symbols

β, thermal expansion coefficient [K^{-1}];
γ, aspect ratio;
θ, angle of inclination;
λ, thermal conductivity [J m^{-1} K^{-1} s^{-1}];
λ_v, width of vortex [m];
μ, viscosity [kg m^{-1} s^{-1}];
ν, kinematic viscosity [m^2 s^{-1}];
ρ, density [kg m^{-3}];
τ, shear stress [Pa];
ψ, stream function of disturbance.

Subscripts and superscripts

C, at the cooled wall or critical condition;
H, at the heated wall;
s, steady state for the undisturbed field;
w, at the wall;
$\langle\ \rangle$, average over the cross-section;
*, dimensional quantity;
', disturbance;
¯, mean over one period in z direction.

1. INTRODUCTION

WHEN a fluid layer between two horizontal parallel plates is heated from below and cooled from above, the buoyancy force normal to the plates makes the flow unstable and gives rise to vortices for a range of Rayleigh number above the critical value (Ra_C = 1708). If forced-flow is superimposed, rolls of longitudinal vortices appear in the fluid layer and enhance the transport processes of heat and momentum.

Mori and Uchida [1] were the first to perform this type of experiment, analyzing the convection by means of a quasi-linear approximation [2–4]. They assumed that, near the critical condition, the disturbance during its growth did not change its spatial cellular pattern; only its amplitude increased. On the basis of energy and entropy-production balances, they determined the amplitude of the disturbance. Their results on the development of the longitudinal vortex and the resultant deformation of the primary-flow fields were in good agreement with the experimental data near the critical condition.

However, in the range of Rayleigh number far above the critical value, non-linear mechanisms prevail and the above assumption cannot account for them adequately. Thus numerical solutions were presented by Ogura and Yagihashi [5] and Hwang and Cheng [6]; the latter pointed out that the increase of the heat transfer coefficient above the result obtained by the quasi-linear approximation reached 25% at a Rayleigh number nine times greater than the critical value. However, in order to discuss further the structure of the vortex in the higher Rayleigh number range, more information from experiments is necessary.

When a fluid layer is bounded by two vertical plates kept at uniform but different temperatures, thermally-driven convection occurs. The flow instability and the dependence of the superimposed forced-flow were investigated experimentally and theoretically by the present authors [7]. It was found that the flow became unstable at a certain Rayleigh number due to a disturbance of a travelling-wave type, the direction of its axis being in the transverse direction and so being different by an angle of $\pi/2$ from that in the horizontal flow case. Thus, a substantial change in the vortex motion occurs as the inclination angle is increased.

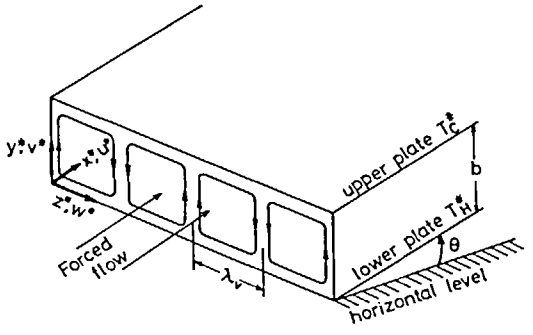

FIG. 1. Flow configuration and coordinate system.

The purpose of the present paper is to present further information on the structure of these vortices in the horizontal flow case in a range of Rayleigh number far above the critical value. Laser–Doppler anemometry was used to measure the flow field. A finite-difference method [8] was applied to predict the flow and temperature fields. The second purpose is to make clear the effect of flow inclination on the primary flow and disturbance pattern. The inclination angle was limited to a maximum of 32.1° from the horizontal; at the maximum inclination, the vortex changed substantially in its structure, although its axis remained parallel to the streamwise direction.

2. THEORETICAL ANALYSIS

2.1. *Governing equations*

Consider a 2-dim. fully-developed laminar flow between inclined parallel plates kept at uniform but different temperatures. Here, it is assumed that the inclination angle θ is small so that the disturbance which causes the flow instability is 2-dim. with its axis in the streamwise direction. The flow configuration and coordinate system are shown in Fig. 1.

Under the Boussinesq approximation, with the reference temperature T_C^* at the cooled wall, the set of governing equations is written as follows:

Continuity equation.

$$\frac{\partial v^*}{\partial y^*} + \frac{\partial w^*}{\partial z^*} = 0. \tag{1}$$

Momentum equations.

$$v^*\frac{\partial u^*}{\partial y^*} + w^*\frac{\partial u^*}{\partial z^*} = -\frac{1}{\rho_C}\frac{\partial p^*}{\partial x^*} + \frac{1}{\rho_C}\nabla(\mu\nabla u^*) + g\beta(T^* - T_C^*)\sin\theta, \tag{2}$$

$$v^*\frac{\partial v^*}{\partial y^*} + w^*\frac{\partial v^*}{\partial z^*} = -\frac{1}{\rho_C}\frac{\partial p^*}{\partial y^*} + \frac{1}{\rho_C}\nabla(\mu\nabla v^*) + g\beta(T^* - T_C^*)\cos\theta, \tag{3}$$

$$v^*\frac{\partial w^*}{\partial y^*} + w^*\frac{\partial w^*}{\partial z^*} = -\frac{1}{\rho_C}\frac{\partial p^+}{\partial z^*} + \frac{1}{\rho_C}\nabla(\mu\nabla w^*). \tag{4}$$

Energy equation.

$$v^*\frac{\partial T^*}{\partial y^*} + w^*\frac{\partial T^*}{\partial z^*} = \frac{1}{\rho_C c_{pC}}\nabla(\lambda\nabla T^*) \tag{5}$$

where $\nabla = \partial/\partial y^* + \partial/\partial z^*$. Here, the axial pressure gradient has been assumed constant over the cross-section and viscous dissipation and compressibility effects in the energy equation have been neglected. In the present analysis, the temperature dependencies of viscosity and thermal conductivity are taken into account.

The following dimensionless variables and parameters are introduced:

$$(x^*, y^*, z^*) = b(x, y, z), \quad (u^*, v^*, w^*) = (u, v, w)\nu_C/b,$$

$$T^* - T_C^* = T(T_H^* - T_C^*), \qquad p^* = p\rho_C\nu_C^2/b^2,$$

$$Gr = g\beta(T_H^* - T_C^*)b^3/\nu_C^2, \qquad Re = \langle u^* \rangle b/\nu_C,$$

$$Gr_x = Gr \sin\theta, \qquad Gr_y = Gr \cos\theta.$$

The dimensionless stream function is defined by

$$v = -\frac{\partial\psi}{\partial z} \quad \text{and} \quad w = \frac{\partial\psi}{\partial y}. \tag{6}$$

Using these dimensionless quantities, the streamwise momentum equation may be expressed by

$$\frac{\partial\psi}{\partial y}\frac{\partial u}{\partial z} - \frac{\partial\psi}{\partial z}\frac{\partial u}{\partial y} = -\frac{\partial p}{\partial x} + \mu/\mu_C \nabla^2 u + \left(\frac{\partial u}{\partial y}\frac{\partial}{\partial y} + \frac{\partial u}{\partial z}\frac{\partial}{\partial z}\right)(\mu/\mu_C) + Gr_x T \tag{7}$$

where $\nabla^2 = \partial^2/\partial y^2 + \partial^2/\partial z^2$. After eliminating the pressure terms from equations (3) and (4), we can derive the following vorticity transport and energy equations:

$$\frac{\partial\psi}{\partial y}\frac{\partial\omega}{\partial z} - \frac{\partial\psi}{\partial z}\frac{\partial\omega}{\partial y} = (\mu/\mu_C)\nabla^2\omega + 2\left(\frac{\partial\omega}{\partial y}\frac{\partial}{\partial y} + \frac{\partial\omega}{\partial z}\frac{\partial}{\partial z}\right)(\mu/\mu_C) - 2\frac{\partial^2\psi}{\partial y\partial z}\frac{\partial^2}{\partial y\partial z}(\mu/\mu_C) - \frac{\partial^2\psi}{\partial y^2}\nabla^2(\mu/\mu_C) + \omega\frac{\partial^2}{\partial z^2}(\mu/\mu_C) + Gr_y\frac{\partial T}{\partial z}, \tag{8}$$

$$\frac{\partial\psi}{\partial y}\frac{\partial T}{\partial z} - \frac{\partial\psi}{\partial z}\frac{\partial T}{\partial y} = \frac{1}{Pr}\left[(\lambda/\lambda_C)\nabla^2 T + \left(\frac{\partial T}{\partial y}\frac{\partial}{\partial y} + \frac{\partial T}{\partial z}\frac{\partial}{\partial z}\right)(\lambda/\lambda_C)\right], \tag{9}$$

where the dimensionless vorticity is defined as

$$\omega = -\nabla^2\psi. \tag{10}$$

The boundary conditions are

$u = \psi = \partial\psi/\partial y = \partial\psi/\partial z = 0$ at $y = 0$ and 1, and at $z = 0$ and γ;

$$T = 1 \text{ at } y = 0 \text{ and } T = 0 \text{ at } y = 1. \tag{11}$$

For the temperature condition at the side walls, we will examine the following two cases:

$$\partial T/\partial y = 0 \quad \text{or} \quad T = 1 - y \quad \text{at } z = 0 \text{ and } \gamma, \tag{12}$$

that is, the adiabatic condition and a linear wall-temperature condition, respectively. It should be noted that, in the present analysis, the width of the vortex has not been specified; it was to be determined for each heat transfer condition and each aspect ratio γ. The variations of viscosity and thermal conductivity are represented approximately as

$$\mu/\mu_C = 1 + a_\mu T, \quad \lambda/\lambda_C = 1 + a_\lambda T. \tag{13}$$

These coupled, nonlinear differential equations (7)–(10), with boundary conditions (11) and (12), will be solved numerically by means of a finite-difference method.

2.2. *Finite-difference equations*

The field of interest is considered to be covered by a linear-orthogonal grid network. The nodes of the finite-difference grid correspond to the intersections of the grid lines. Figure 2 shows a typical node P, four surrounding nodes N, S, E and W, and nodes labelled NE, NW, SE and SW. Following the procedure of Gosman *et al.* [8], equations (7)–(10) are expressed in finite-difference form. For example,

$$u_P = \{u_E(A_E + B_U) + u_W(A_W + B_U) + u_N(A_N + B_U) + u_S(A_S + B_U) - h^2 dp/dx + Gr_x T_P h^2 + 0.25a_\mu \times [(T_N - T_S)(u_N - u_S) + (T_E - T_W)(u_E - u_W)]\} /[A_E + A_W + A_N + A_S + 4B_U] \tag{14}$$

where

$$A_E = [(\psi_{SE} + \psi_S - \psi_{NE} - \psi_N) + |\psi_{SE} + \psi_S - \psi_{NE} - \psi_N|]/8, \tag{15}$$

and so on.

$$B_U = 1 + a_\mu T_P, \quad B_T = 1 + a_\lambda T_P. \tag{16), (17}$$

If viscosity and thermal conductivity are presumed constant,

$$a_\mu = a_\lambda = 0.$$

In the numerical calculation the space subscripts in the finite-difference equations such as equation (14) are replaced by i and j in the y and z directions, respectively.

Expressions for the surface vorticity were obtained by use of a Taylor expansion out from the wall and by neglecting terms of more than the second order. For example, the boundary conditions at the lower plate may be written as

$$u_{1,j} = \psi_{1,j} = 0, \; T_{1,j} = 1, \; \omega_{1,j} = (8\psi_{2,j} - \psi_{3,j})/2h^2 \quad \text{at } y = 0. \tag{18}$$

Here $i = 1, 2, \ldots, M$ and $j = 1, 2, \ldots, N$.

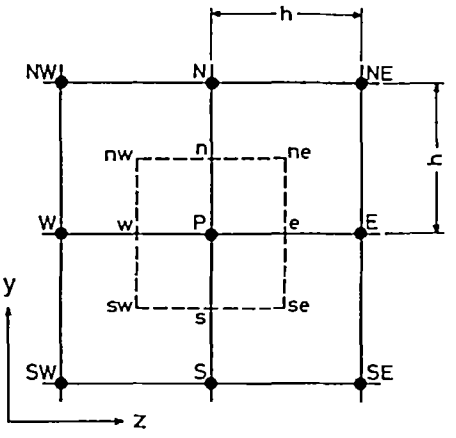

FIG. 2. Finite-difference grid; broken lines enclose area of integration [8].

2.3. *Method of solution*

In addition to the above equations, another constraint is required from the conservation of total mass,

$$Re = \langle u^* \rangle b/\nu_C = \int_0^\gamma \int_0^1 u \, dy \, dz/\gamma. \quad (19)$$

Of the four parameters *Re*, *Gr*, *Pr* and d*p*/d*x* in the governing equations, all except d*p*/d*x* were used as input data.

Numerical calculations were performed by an under-relaxation method and a point-iterative procedure. First, distributions of temperature, stream function and vorticity were determined simultaneously from equations (8)–(10), in which the streamwise velocity does not appear. Next, equation (7) was solved for the streamwise velocity. Finally, d*p*/d*x* was determined to satisfy constraint (19).

In the numerical calculations, the number of grid lines was selected as $M = 21$ and $N = 401$. For the square grid adopted, the aspect ratio was 20, corresponding to the experiment to be described later. Other values of M and N, e.g. $M = 11$ and $N = 201$ and $M = 41$ and $N = 801$ were also tested for flow conditions of (Re, Gr, θ) = (200, 5100, 0) and (46.2, 7400, 0), and the selected values of M and N were judged to be large enough. The calculation was terminated when the changes of all variables in successive iterations became less than 0.1%.

3. EXPERIMENTAL APPARATUS AND PROCEDURE

The experimental apparatus is shown schematically in Fig. 3. The experiment was performed in a rectangular duct with a large aspect ratio. The duct was 2 m long, its cross-section being 0.200 m × 0.011 m; it could be set at an arbitrary inclination angle θ from the horizontal. The heat transfer surfaces were made of 3 mm thick stainless steel plates. Behind them jackets were attached through which cooled water and steam, respectively, flowed to maintain the heat transfer surfaces at uniform temperatures. The side walls were made of 10 mm thick wooden (adiabatic) plates.

The test fluid was air which was circulated in the closed flow system. Measurements were made at the cross-section 1.6 m downstream of the entrance, i.e. 73 hydraulic diameters downstream. This long entrance length, as well as the maintenance of the entrance temperature the same as the outlet temperature, was sufficient to establish the fully-developed flow and temperature fields at the measuring section. For the measurement of very low velocities, a laser–Doppler velocimeter (Kanomax Type 27) was used in the fringe mode. The beam intersection angle was 18.9°. The intersection point was moved vertically and laterally by a traversing system. Smoke was generated using an incense stick placed in the mixing box just upstream of the duct entrance. This permitted the visualization of the flow pattern and provided seeding for the laser–Doppler velocimetry. Simultaneous measurements of the temperature patterns were performed by means of a sheathed Ar–Cr thermocouple of 0.25 mm O.D. The heat transfer rates at the walls were determined from the temperature gradients near the walls.

The cross-sectional mean velocity $\langle u^* \rangle$ ranged from 0.029 to 0.14 m s^{-1}, so that the Reynolds numbers Re were in the range 17.0–80.1. The temperature difference between the plates was less than 85 K and the Grashof numbers Gr ranged from 2700 to 9300. The inclination angle θ was varied from 0 to 32.1° from the horizontal. The lower plate was always heated.

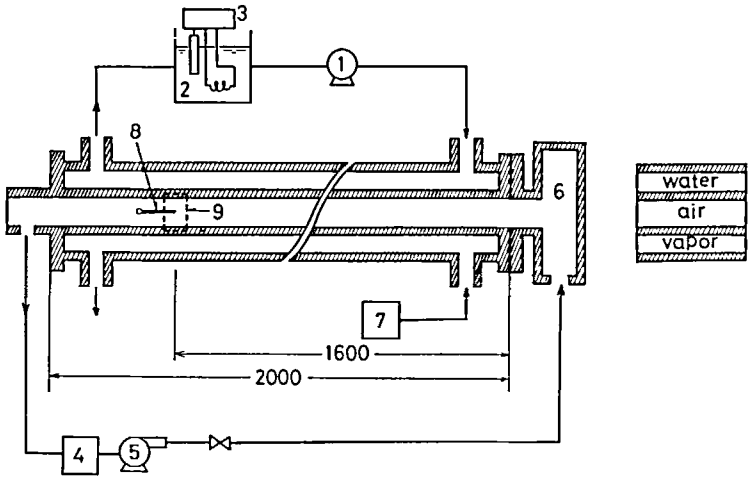

FIG. 3. Schematic diagram of the experimental apparatus; 1 pump, 2 tank, 3 temperature controller, 4 air tank, 5 blower, 6 mixing box, 7 vapor generator, 8 thermocouple, 9 optical glass.

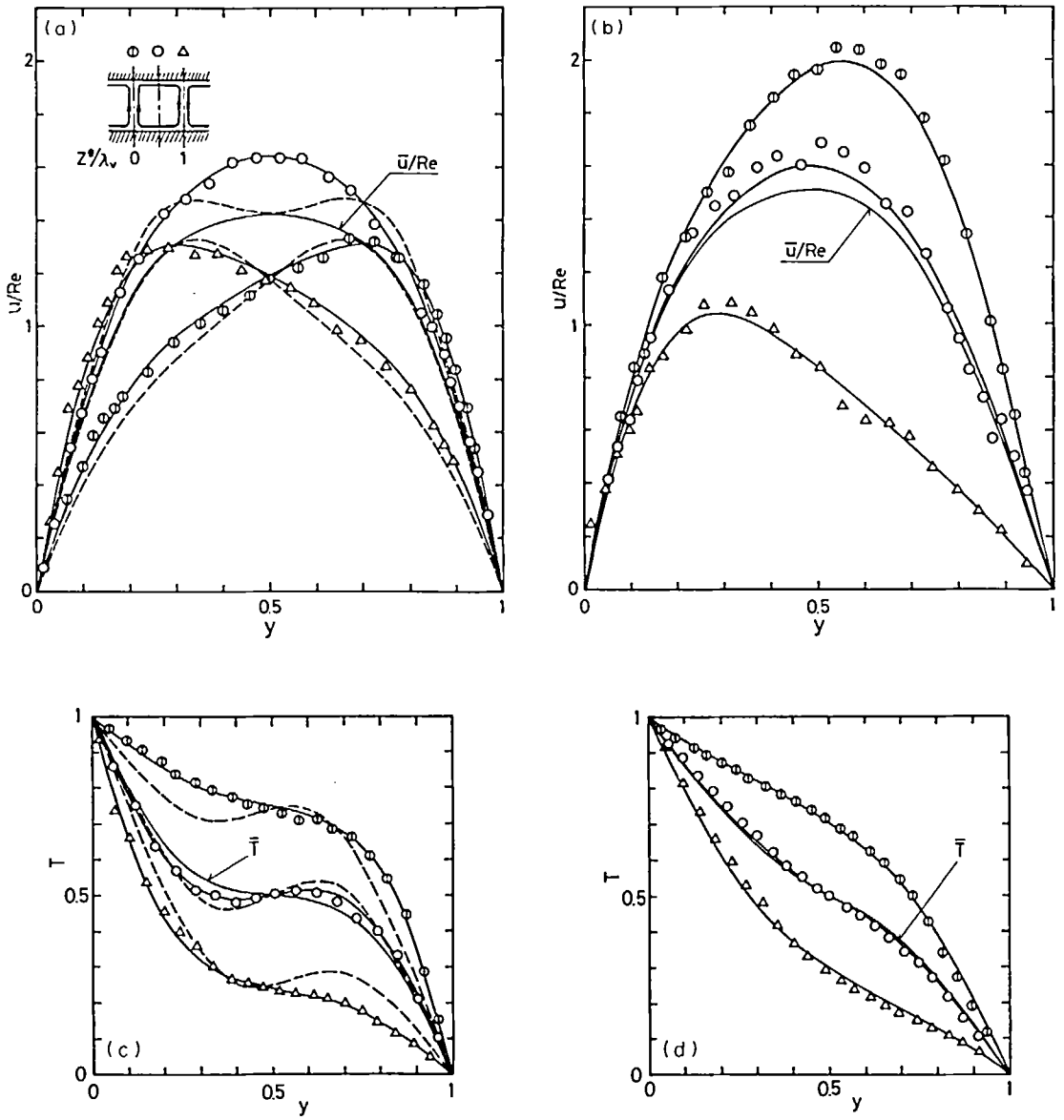

FIG. 4. Distributions of longitudinal velocity and temperature in the y direction. ——; Numerical prediction, ---; analytical solution of Mori *et al.* [1]. (a) and (c); $Re = 46.2$, $Gr = 7400$ and $\theta = 0°$, (b) and (d); $Re = 46.2$, $Gr_y = 3770$ and $\theta = 32.1°$.

4. RESULTS AND DISCUSSION

4.1. *Effects of variable properties and boundary conditions*

Since the aspect ratio is very large, the flow in the central region of the duct may be assumed to be the same as that between infinite parallel plates. Here and in the following sections the discussion will be limited to the flow in the central region of the duct.

In the horizontal flow case, if the temperature dependencies of viscosity, thermal conductivity and density are taken into account, the numerical calculation predicts that the absolute values of the vorticity and stream function would be decreased by about 10% when the temperature difference between the plates attains 52 K ($Gr = 7400$). However, when they are normalized by their maximum values, changes in the vorticity and stream function patterns over the cross-section are very small. Changes in the longitudinal velocity, temperature and vortex width are less than 1%. Therefore, the structure of the vortex is considered to be unaffected by the temperature dependencies of the physical properties in the present experimental conditions. This is also true in the inclined flow case.

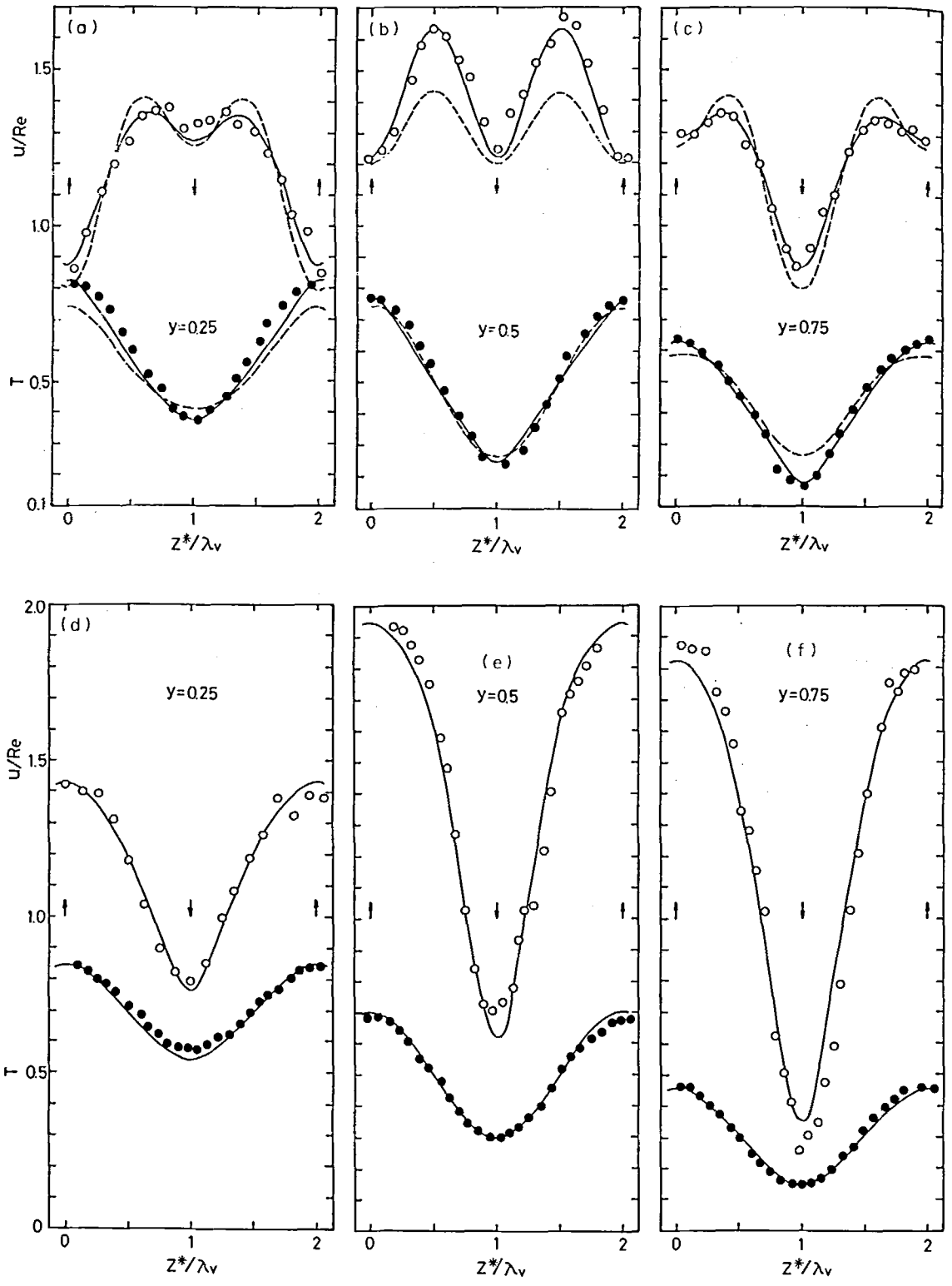

FIG. 5. Lateral distributions of longitudinal velocity and temperature. Details as Fig. 4. Arrows show boundaries of vortices. (a)-(c); $Re = 76.4$, $Gr = 6522$ and $\theta = 0°$, (d)-(f); $Re = 46.2$, $Gr_y = 3770$ and $\theta = 32.1°$.

It is sometimes the case in thermal convection problems that different initial perturbations produce different mode solutions when approaching steady state. We compared solutions using (a) uniform profiles of velocity and temperature and (b) profiles with different external conditions. (Calculated in the previous step of execution.) These gave substantially the same result. Also, two boundary conditions at the side walls were examined; (a) the adiabatic condition and (b) linear-temperature condition. These agreed to within an error of 0.6% in the region far from the side walls, at least at an aspect ratio 20.

Thus, only the results with constant properties and a linear temperature profile at the side walls will be discussed in the following sections.

4.2. *Horizontal flow case*

As mentioned before, there have been analytical and numerical investigations of the flow pattern and structure of the longitudinal vortex motion in the supercritical condition. However, the results have only been compared against the experimental results of Mori and Uchida [1]. As for the longitudinal velocity field, Ogura and Yagihashi [5] and Hwang and Cheng [6] as well as the present investigation, have predicted accurately the experimental results of Mori and Uchida at $Ra = 8010$ ($= 4.69\,Ra_C$). However, they have failed to predict accurately the measured temperature distributions. Ogura and Yagihashi examined the numerical calculation and experimental data in detail, and discussed reasons for the discrepancy. Later Ostrach and Kamotani's [9] heat transfer experiment showed that, for $Ra > 8000$ (the same range as that used by Mori and Uchida), stable vortex rolls disappeared and the fluid motion became irregular. They also detected a reversal of the mean temperature gradient in the central region of the channel. That counter-gradient heat flux (advected by the vortex motion) had not been observed by Mori and Uchida, but it was predicted numerically as well as analytically.

Presented here are the experimental results of the present investigation. The distributions of longitudinal velocity and temperature in the y direction are shown in Figs. 4(a) and (b) and those in the spanwise direction are shown in Figs. 5(a)–(c). Here and in the following sections the origin of z^* was shifted to the upwelling boundary of the vortex near the center. In Fig. 4, profiles of the mean velocity $\bar{u}$ and temperature $\bar{T}$ are also shown. The present experiment shows clearly the counter-gradient heat flux in the central region of the vortex, as seen in the profile of local temperature at $z^*/\lambda_v = 0.5$ [open circles in Fig. 4(b)]. The numerical predictions as well as the analytical solutions of Mori and Uchida are also shown in these figures. The numerical prediction agrees well with the experimental results. Thus, we conclude that the numerical results represent the real flow field in the supercritical condition, at least in so far as the vortex motion remains stable and 2-dim., i.e. at $Ra < 8000$.

In contrast to this, the analytical solution appears valid only in the region of Rayleigh numbers not very much larger than the critical value. Hwang and Cheng [6] estimated the limitation of Rayleigh number to be less than 3000, in so far as the heat transfer rate was concerned. As seen in Fig. 4, the analytical solution shows a concave profile of longitudinal velocity near the center of the vortex. It also overpredicts a large positive temperature gradient in the central region of the channel. These discrepancies increase with increasing the Rayleigh number. This is supposedly due to the fact that the analytical solution does not account sufficiently for the nonlinear effects of the vortex motion.

Isopleths of longitudinal velocity and isotherms of the primary flow field are shown in Figs. 6(a) and 7(a), respectively. The velocity peak appears near the center of the vortex, where the isopleths incline upward in the upwelling region. This results in a drastic change of the lateral distribution of u/Re (Fig. 5). Isotherms for both the primary flow and disturbance [Fig. 7(a)] and the streamlines [Fig. 7(b)] show clearly that a positively buoyant plume rises up in the plane $z^*/\lambda_v = 0$. It impinges upon the upper plate and spreads laterally. At the other boundaries (i.e. $z^*/\lambda_v = \pm 1$) negatively buoyant plumes arise. This regular alignment of the plumes constitutes the longitudinal vortex motion and these plumes block the primary flow significantly (see the isopleths of $u'/|u'|_{max}$). Here it should be noted that u' and T' were obtained as deviations from mean values, $\bar{u}$ and $\bar{T}$, respectively.

4.3. *Inclined flow case*

In the first case to be discussed, the fluid flows upward between the parallel plates, the lower plate being heated and the upper one cooled. As the fluid layer is inclined from the horizontal, the thermally-driven motion is superimposed on the forced flow. The primary flow field in the subcritical condition is represented by the steady solution of equation (2) as

$$u_s = (Gr_x - 24\,Re)\,(y^2 - y)/4 + Gr_x(y^3 - 3y^2 + 2y)/6. \quad (20)$$

However, in the supercritical condition, the vortex motions significantly disturb the primary flow fields, which are very different from those in the horizontal flow case. The measured distributions of longitudinal velocity and temperature in the y direction are shown in Fig. 4 for an inclination angle θ of 32.1°.

When the fluid layer is inclined, upwelling caused by the positively buoyant plume of the vortex has a positive velocity component in the flow direction, which results in increasing the longitudinal velocity at the vortex boundary $z^*/\lambda_v = 0$, while downwelling due to the negatively buoyant plume works to reduce the flow at the other vortex boundary. This results in the remarkably skewed profile of the longitudinal velocity. In contrast to this, if Gr_y is constant [see equations (8)–(10)], the temperature field, as well as ψ and ω, does not change with θ.

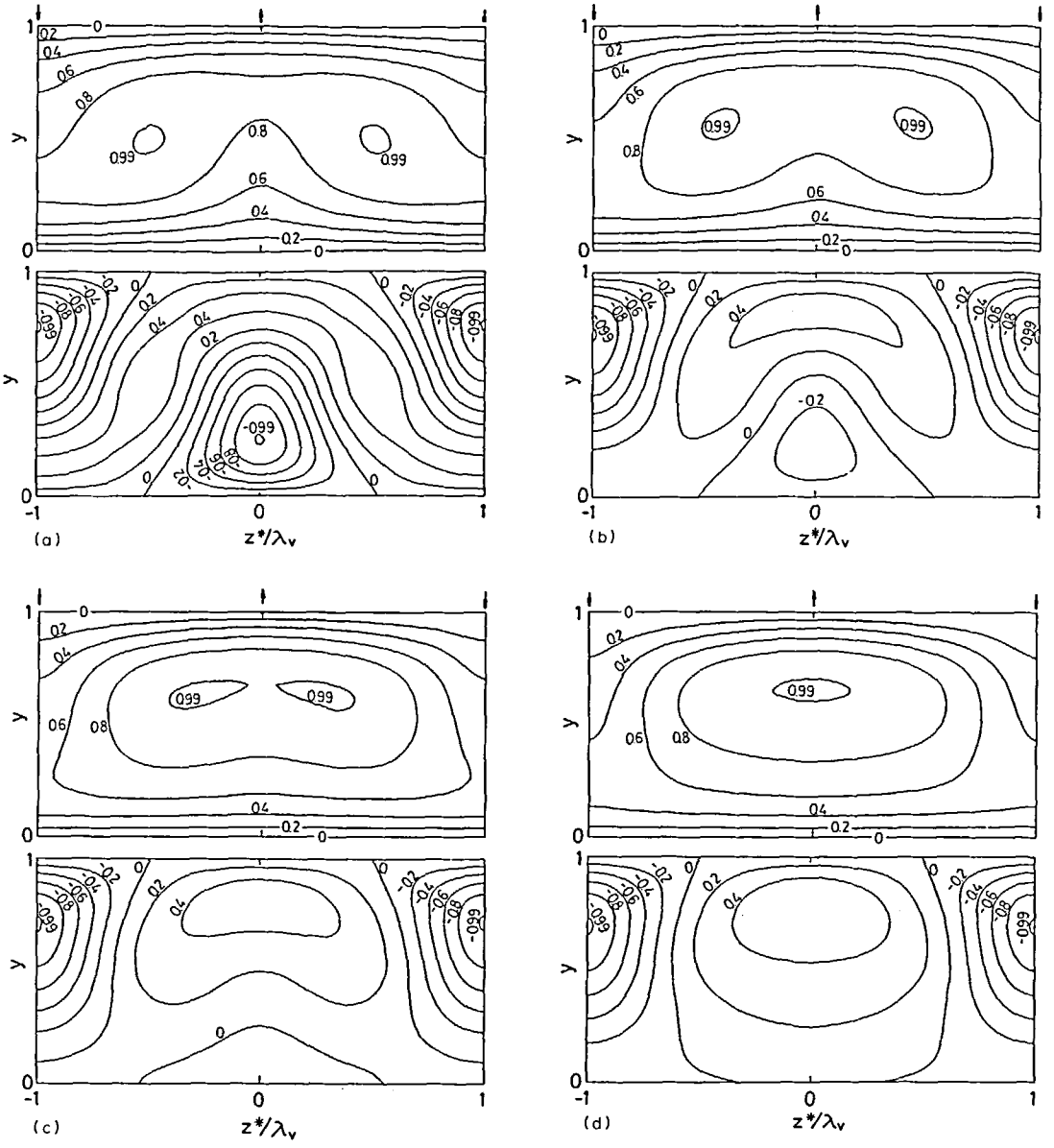

FIG. 6. Change of the primary flow (u/u_{max}, upper row) and disturbance pattern ($u'/|u'|_{max}$, lower row) with flow inclination at $Re = 46.2$ and $Gr_y = 7400$. (a); $\theta = 0°$, (b); $\theta = 10°$, (c); $\theta = 20°$, (d); $\theta = 30°$.

A remarkable change may also be seen in the lateral distributions. For example, in Fig. 5 it is obvious that the amplitude of variation of the longitudinal velocity is small near the lower plate but becomes significantly larger in the upper-half region. Moreover, the two vortices in a pair cannot be distinguished, since they share a single peak.

Such a change in the primary flow field with flow inclination can be understood intuitively from the isopleths of u (Fig. 6); in the horizontal flow case, the velocity peaks are located near the center of each vortex. These peaks approach the upwelling boundary between vortices as the inclination angle increases positively. Ultimately the two peaks merge into one. Thus a single velocity peak appears at the upwelling boundary of a pair of vortices, and the minimum velocity is observed at the other boundary. Disturbance patterns of the longitudinal velocity are also shown in Fig. 6. It can be clearly seen that the acceleration caused by the upwelling of the positively-buoyant plume overcomes the flow-blockage due to the plume itself at $\theta = 30°$.

When the fluid flows downward between parallel plates (inclination angle θ negative), the thermal forces tend to retard the primary flow near the lower plate and enhance it near the upper plate. Thus the primary flow has a velocity profile that is skewed toward the upper plate, in contrast to the case with positive θ. [See equation (20) for the subcritical condition.] This is also true in the secondary flow due

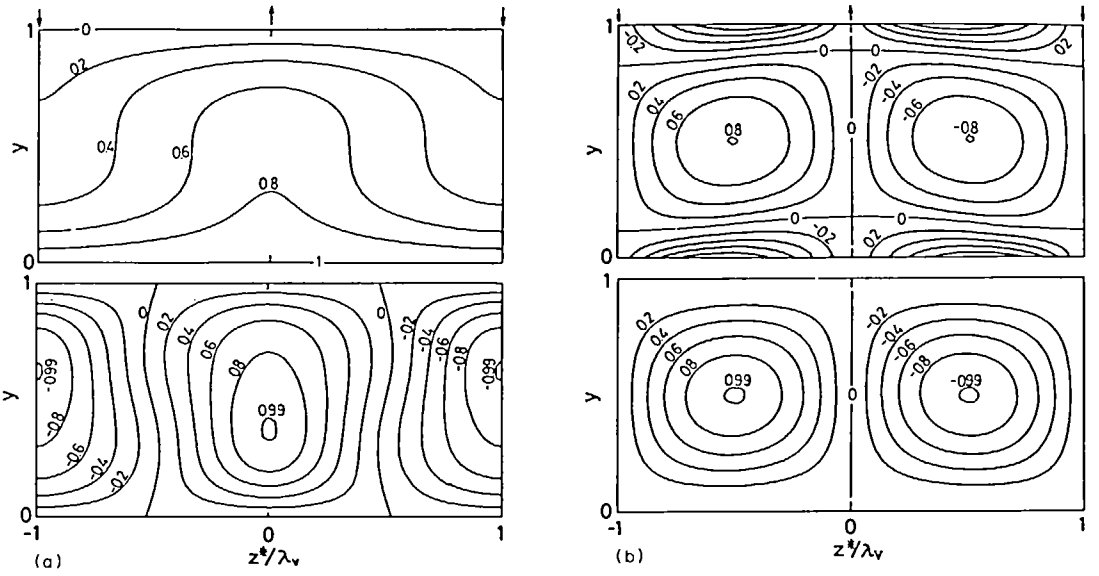

FIG. 7. Patterns of primary flow and disturbance in the horizontal flow case at $Re = 46.2$ and $Gr = 7400$. (a); Isotherms (T) in the primary flow field (upper row) and those of $T/|T'|_{max}$ (lower row), (b) · isovorticity lines of $\omega/|\omega|_{max}$ (upper) and streamlines of $\psi/|\psi|_{max}$ (lower).

to the vortex motion; that is, the upwelling caused by the positively-buoyant plume works to retard the primary flow and the negatively buoyant plume accelerates it. This plume action is just contrary to the case with positive θ. Therefore, the patterns of the primary flow and disturbance are found to be like those of Fig. 6, except they are now inverted; that is, the velocity peaks which were located at the vortex centers in the horizontal flow case approach the downwelling boundary of the vortex pair and finally merge.

4.4. *Nusselt number*

In the fully developed condition heat flows across the fluid layer. Thus the Nusselt number is defined as the dimensionless temperature gradient averaged over the vortex width

$$\overline{Nu} \equiv qb/\lambda\,(T_H^* - T_C^*) = \overline{|dT/dy|}_w. \qquad (21)$$

All the numerical results for the horizontal flow case and for the inclined flow case with positive and negative θ fall on a single curve when plotted against Ra_y/Ra_C, where Ra_y is the Rayleigh number based on the buoyancy force perpendicular to the plates. These are presented in Fig. 8 together with the results of the present and previous experiments. In the region of Rayleigh number larger than its critical value, the heat transfer rate is enhanced significantly by the vortex motion. The numerical results represent accurately the heat transfer augmentation observed experimentally in the present investigation and by Ostrach and Kamotani [9].

In the region of Rayleigh numbers not very much larger than the critical value, the augmentation of the Nusselt number is well represented by the analytical solution given by Mori and Uchida [1]

$$Nu = 1 + 1.413\,[1 - (Ra_C/Ra_y)] \qquad (22a)$$

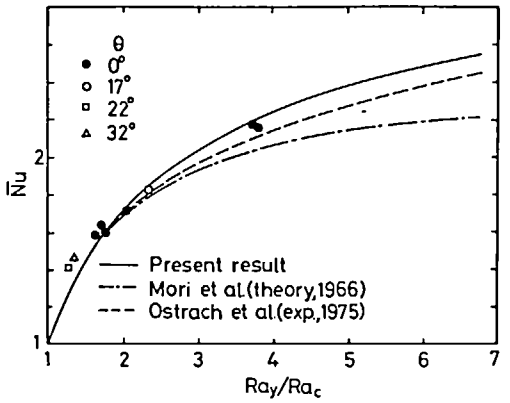

FIG. 8. Averaged Nusselt number in the supercritical condition in both the horizontal and inclined flow cases.

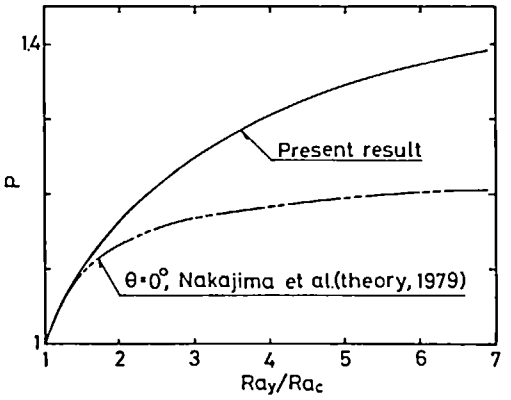

FIG. 9. Normalized pressure gradient p in the supercritical condition in both the horizontal and inclined flow cases.

or

$$(Ra_y/Ra_C)\,Nu - 1 = 2.413\,[(Ra_y/Ra_C) - 1]. \quad (22b)$$

When the Rayleigh number is 1.7 times the critical value, the analytical solution tends to deviate from the numerical solution. This deviation becomes larger with increasing Rayleigh number. In the region of larger Rayleigh numbers ($2 < Ra_y/Ra_C < 6$), the Nusselt number may be expressed accurately by

$$Nu = 1.43\,(Ra_y/Ra_C)^{1/3}, \quad (23)$$

which suggests that the heat transfer rate is independent of the length scale b. A similar relation has been predicted on the basis of dimensional analysis for Bénard convection at large Rayleigh numbers and has been verified experimentally and numerically, although the proportionality constant (e.g. the value 0.83 has been obtained [10]) is 58% smaller than the value for the present case of combined free and forced convection.

Another formulation can be made in the form of equation (22b). From his numerical calculation of finite-amplitude Bénard convection with free boundaries, Veronis [11] presented the following empirical relation for the range of $2 < Ra_y/Ra_C < 6$:

$$(Ra_y/Ra_C)\,Nu - 1 \propto (Ra_y/Ra_C - 1)^{1.15}. \quad (24)$$

For that range of Rayleigh number, the present numerical calculation predicts a power of 1.11, which compares well with the value of Veronis. A compromise formula, valid over the whole range of Rayleigh number examined, i.e. $1 \leqslant Ra_y/Ra_C \leqslant 6$, is

$$(Ra_y/Ra_C)\,Nu - 1 = 2.47\,(Ra_y/Ra_C - 1)^{1.07}. \quad (25)$$

This formula predicts the Nusselt number within an error of less than 3%.

4.5. *Pressure drop*

In the subcritical condition the friction factors and the pressure drop are obtained from the steady solution as

$$(f_{\mathrm{II}}, f_C) = 12/Re + Gr_x/Re^2\,(1, -1)/6, \quad (26)$$

$$dp_0/dx = -Re^2\,(f_{\mathrm{II}} + f_C)/2 = -12\,Re. \quad (27)$$

Here, it should be noted that the static pressure p_0 is referred to that at the center of the fluid layer.

In the supercritical condition the pressure drop increases with the Rayleigh number. In their analysis based on the quasilinear approximation, Mori and Uchida [1] presumed that $dp_0/dx = -12/Re$. But, by retaining the nonlinear terms in the momentum equations and making use of the quasilinear approximation, we can obtain the following expression in the horizontal flow case [12]:

$$p - 1 = [(Ra_y/Ra_C) - 1]/\{4.294[(Ra_y/Ra_C) - 1] + 6.368\,Pr^2\} \text{ where } p = -[(dp_0/dx)/12]Re. \quad (28)$$

This equation together with the numerical results are presented in Fig. 9. A sharp increase of the pressure drop across the critical Rayleigh number is observed. This increase, however, is not as large as that of the Nusselt number. The analytical solution (28) gives a good approximation for the pressure drop over the range of Rayleigh number not very much larger than the critical value, i.e. for $Ra_y/Ra_C < 1.4$.

With increasing inclination angle θ, the structure of the vortex motion changes drastically, but the increase of the pressure drop is approximately independent of θ. This is similar to the case of the heat transfer process. The increase of the pressure drop obtained numerically may be represented, in a form similar to equation (25), by

$$(Ra_y/Ra_C)\,p - 1 = 1.345\,(Ra_y/Ra_C - 1)^{1.048}, \quad (29)$$

in which the maximum error is less than 3% for the whole range of Rayleigh number examined, i.e., $1 \leqslant Ra_y/Ra_C \leqslant 6$.

5. CONCLUSIONS

Laminar flow between horizontal and inclined parallel plates heated from below and cooled from above was investigated experimentally and theoretically for the range of Rayleigh number Ra above the critical value, $Ra_C = 1708$. Experiments were performed by use of a laser–Doppler anemometer and thermocouple. Theoretical predictions were made by means of a finite-difference method. The longitudinal vortex and its effects on the transport processes were examined and the following results were obtained:

(1) For the horizontal flow case, a new experimental data set is provided which confirmed that the numerical prediction does represent the real flow and temperature fields in the Rayleigh number range above the critical value, at least as far as stable and 2-dim. vortex motion exists (i.e. for Rayleigh numbers less than 8000). The main difference from the experimental data published hitherto is the temperature field; the local temperature profiles of the present experiments show a reversal of the temperature gradient in the central region of the flow, that is, a counter-gradient heat flow which arises due to the advective motion of the longitudinal vortex.

The analytical solution of the integral energy equations gives a good approximation in the Rayleigh number region not very much above the critical value. But at larger Rayleigh number, it fails to predict the real flow due to the fact that it does not account sufficiently for the nonlinear effect caused by the vortex motion.

(2) When the fluid layer is inclined from the horizontal, the positively- and negatively-buoyant plumes, of which the vortex motion is composed, affect the primary-flow directly; in the upward-inclined flow, the downwelling of the negatively buoyant plume works to retard the primary-flow and the upwelling does the opposite. The velocity peaks are located near the

center of each vortex in the horizontal flow case; they move toward the upwelling boundary of the vortex pair as the inclination-angle is increased, and ultimately they merge to form one peak at the upwelling boundary. Thus a single peak appears for a pair of vortices. In the downward-inclined flow, the patterns of the primary flow and disturbance are inverted from those in the upward flow.

(3) Sharp increases of the Nusselt number and pressure drop are observed across the critical Rayleigh number. At large Rayleigh numbers, the heat transfer rate becomes independent of the length scale. The augmentations of Nusselt number and pressure drop become independent of inclination angle, although the augmentation of the pressure drop is smaller. They are represented by equations (25) and (29), respectively, for the whole range of Rayleigh number examined, i.e. for $Ra_y/Ra_C \leqslant 6$.

REFERENCES

1. Y. Mori and Y. Uchida, Forced convective heat transfer berween horizontal flat plates, *Int. J. Heat Mass Transfer* **9**, 803–817 (1966).
2. K. Gotoh and M. Satoh, The stability of a natural convection between two parallel vertical planes, *J. Phys. Soc., Japan* **21**, 542–548 (1966).
3. J. T. Stuart, On the non-linear mechanics of hydrodynamic stability, *J. Fluid Mech.* **4**, 1–21 (1956).
4. J. T. Stuart, On the role of Reynolds stresses in stability theory, *J. Aero. Sci.* **23**, 86–88 (1956).
5. Y. Ogura and A. Yagihashi, A numerical study of convection rolls in a flow between horizontal parallel plates, *J. Met. Soc., Japan* **47**, 205–217 (1969).
6. G. T. Hwang and K. C. Cheng, A boundary vorticity method for finite amplitude convection in plane Poiseuille flow, *Proc. 12th Midwestern Mechanics Conf.*, Univ. of Notre Dame, Vol. 6, pp. 207–220 (1971).
7. K. Fukui, M. Nakajima, H. Ueda and T. Mizushina, Flow instability and transport phenomena in combined free and forced convection between vertical parallel plates, *J. Chem. Engng, Japan* **15**, 172–180 (1982).
8. A. D. Gosman, W. M. Pun, A. K. Rumchal, D. B. Spalding and M. Wolfshtein, *Heat and Mass Transfer in Recirculating Flows*. Academic Press, New York (1969).
9. S. Ostrach and Y. Kamotani, Heat transfer augmentation in laminar fully developed channel flow by means of heating from below, *Trans Am. Soc. Mech. Engrs*, Series C, *J. Heat Transfer* **97**, 220–225 (1975).
10. S. Globe and D. Dropkin, Natural-convection heat transfer in liquids confined by two horizontal plates and heated from below, *Trans Am. Soc. Mech. Engrs*, Series C, *J. Heat Transfer* **81**, 24–28 (1959).
11. G. Veronis, Large-amplitude Bénard convection, *J. Fluid Mech.* **26**, 49–68 (1966).
12. M. Nakajima, K. Fukui, T. Uchida, H. Ueda and T. Mizushina, Secondary flow in combined free and forced convection between inclined parallel plates, 13th Autumn Meeting of Soc. Chem. Eng. Japan, Nagoya, D201, pp. 266–267 (1979).

TOURBILLON LONGITUDINAL ET SES EFFETS SUR LES MECANISMES DE TRANSPORT EN CONVECTION LAMINAIRE MIXTE ENTRE DES PLAQUES PARALLELES HORIZONTALES OU INCLINEES

Résumé—On étudie le tourbillon longitudinal et ses effets sur les mécanismes de transport en écoulement lainaire entre des plaques parallèles horizontales ou inclinées, maintenues à des températures différentes. On présente une nouvelle série d'expériences et de résultats sur les champs de vitesse et de température. Des calculs théoriques sont effectués au moyen d'une méthode numérique aux différences finies. A partir d'un bon accord entre théorie et expérience, les champs de perturbation de l'écoulement primaire et les configurations de perturbation sont examinés pour les écoulements horizontaux et inclinés. L'angle d'inclinaison est au maximum de 32,1° à partir de l'horizontale et les nombres de Rayleigh sont inférieurs à 9300. On constate que l'interaction entre les tourbillons sont faibles dans l'écoulement horizontal, le pic de vitesse étant proche du centre du tourbillon. Dans l'écoulement incliné, les configurations de perturbation changent beaucoup ; deux tourbillons voisins tendent à former une paire qui a un seul pic de vitesse à la frontière montante du tourbillon dans l'écoulement ascentionnel, et au contraire à la frontière descendante dans l'écoulement descendant. Des augmentations du nombre de Nusselt et de la chute de pression dues à la formation de tourbillons sont indépendantes de l'angle d'inclinaison et sont formulées de façon simple.

LÄNGSWIRBEL UND IHR EINFLUSS AUF DIE ÜBERTRAGUNGSVORGÄNGE BEI GEMISCHTER FREIER UND ERZWUNGENER LAMINARER KONVEKTION ZWISCHEN WAAGERECHTEN UND GENEIGTEN PARALLELEN PLATTEN

Zusammenfassung—Die Längswirbel und ihr Enfluß auf übertragungsvorgänge in laminarer Strömung zwischen waagerechten und geneigten parallelen Platten mit unterschiedlicher konstanter Temperatur wurden untersucht. Es werden neue experimentelle Daten über die Geschwindigkeits- und Temperaturfelder vorgelegt. Theoretische Berechnungen wurden mit einem numerischen Differenzenverfahren durchgeführt. Auf der Grundlage der guten Übereinstimmung zwischen Theorie und Experiment wurden die gestörten Primärströmungsfelder mit ihren Störungsmustern sowohl für horizontale wie auch geneigte Strömungen untersucht. Der Neigungswinkel betrug maximal 32,1° gegen die Horizontale und die Rayleigh-Zahl lag unterhalb 9300. Es zeigte sich, daß die Wechselwirkung zwischen den Wirbeln bei der horizontalen Strömung sehr gering war, wobei das Geschwindigkeitsmaximum nahe dem Wirbelzentrum lag. In der geneigten Strömung dagegen änderten sich die Störungsmuster erheblich ; zwei benachbarte Wirbel neigten zur Paarbildung mit einem Geschwindigkeitsmaximum an der oberen Wirbelgrenze bei Aufwärtsströmung und umgekehrt an der unteren Grenze bei Abwärtsströmung. Es wird gezeigt, daß das Anwachsen der Nußelt-Zahl und des Druckabfalls infolge der Wirbelbildung unabhängig vom Neigungswinkel ist und in einfacher Form ausgedrückt werden kann.

ПРОДОЛЬНЫЙ ВИХРЬ И ЕГО ВЛИЯНИЕ НА ПРОЦЕССЫ ПЕРЕНОСА ПРИ СМЕШАННОЙ СВОБОДНОЙ И ВЫНУЖДЕННОЙ ЛАМИНАРНОЙ КОНВЕКЦИИ МЕЖДУ ГОРИЗОНТАЛЬНЫМИ И НАКЛОННЫМИ ПАРАЛЛЕЛЬНЫМИ ПЛАСТИНАМИ

Аннотация—Проведено исследование поведения продольного вихря и его влияния на процессы переноса при ламинарном течении между горизонтальными и наклонными параллельными пластинами, имеющими разную температуру. Получены новые экспериментальные данные по полям скорости и температуры. Проведены теоретические расчеты с помощью численного конечно-разностного метода. На основе хорошего совпадения результатов теоретического расчета с экспериментальными данными выполнено исследование возмущенных полей первичного потока и картин возмущения как при горизонтальном, так и наклонном течениях. Максимальный угол наклона составлял '32,1°, а значения числа Рэлея не превышали 9300. Показано, что вихри взаимодействуют намного слабее при горизонтальном течении, причем пик скорости находится у центра вихря. При наклонном течении картины возмущения существенно изменяются: два соседних вихря стремятся образовать пару, у которой пик скорости находится на верхней границе вихря при направленном вверх течении и, наоборот, на нижней границе при направленном вниз течении. Показано, что увеличение числа Нуссельта и перепада давления при образовании вихрей не зависит от угла наклона. Предложена простая по форме зависимость.